Proceedings of the 21st ICSMGE, Vienna, Austria, 14 – 19 June 2026. Pistrol, Adam & Schweiger (eds.)
Published by: ÖGG, Austrian Society for Geomechanics, Salzburg, Austria, ISBN 978-3-9503898-4-5
https://doi.org/10.53243/ICSMGE2026-2355

Numerical technique of coupling peridynamics-DEM and its extension to tensile fracture of compacted clay

Yutaka Fukumoto
Okayama University, Japan, yutakafukumoto@okayama-u.ac.jp

Taiki Shimbo
National Institute of Technology, Ishikawa College, Japan

ABSTRACT: The study proposed a 3-D combined model of peridynamics (PD) and the discrete element method (DEM) to continuously handle the process of the failure of compacted clay. The bond-based model of PD is employed to reproduce the behavior from the initiation of cracks to fracture. At the same time, the DEM is introduced to calculate the interaction forces, including friction, between fragmented pieces after fracture. Additionally, a bilinear bond softening model was introduced to obtain a nonlinear stress–strain relationship, which is often observed in compacted clay. The proposed model was validated by comparing experimental and numerical results of the diametral compression test of compacted clay specimens with a single initial crack. Simulations of compressive failure of multiple crushable objects, representing compacted clay, were also conducted to show the effectiveness of the coupled PD-DEM model.

KEYWORDS: Computational geomechanics, Peridynamics, DEM, Crack propagation.

1 INTRODUCTION

Numerical modeling of fractures, including crack propagation, is a critical problem pertaining to various geomaterials. Soils, which are generally cohesive-frictional granular materials formed under compacted, frozen, or cement-amended conditions, are susceptible to fracture due to the tensile failure. Unlike other construction materials such as concrete, the soil is fragile and exhibits complex fracture and post-fracture behavior. To properly simulate the post-fracture behavior, it is important to consider the cyclic process of soil deformation followed by crack merging-propagation, and contact between newly developed fractured surface in an efficient manner. It is also important to ensure that the cohesive-frictional material properties are properly reflected in the numerical framework.

This study describes a 3-D coupled peridynamics (PD) and discrete element method (DEM) that can handle both the fracture and the post-fracture behavior simultaneously (Fukumoto and Shimbo, 2023). This model is employed in PD to reproduce the behavior from the initiation of cracks to the fracture. At the same time, the DEM is also introduced so that the interaction forces between the fragmented pieces after the fracture can be calculated including the frictional contact forces. The other objective of this study is to simulate the tensile failure behavior of compacted clay. A bond softening model was introduced to capture the nonlinear stress-strain relationship often observed in compacted clay. The proposed PD-DEM model was validated by comparing the experimental results with the numerical simulations of the diametral compression test of compacted clay specimens with a single initial crack. Additionally, simulations of compressive failure of multiple crushable objects, representing compacted clay, were conducted.

2 NUMERICAL MODEL

2.1 *Coupling PD and DEM*

PD is a non-local, continuum-based, mesh-free method, which is good at handling cases where cracks branch or where multiple cracks propagate simultaneously. In this study, the bond-based PD model (BB-PD) was adopted. Although it has more constraints compared to the ordinary state-based PD model (OSB-PD), its computational process is simpler and

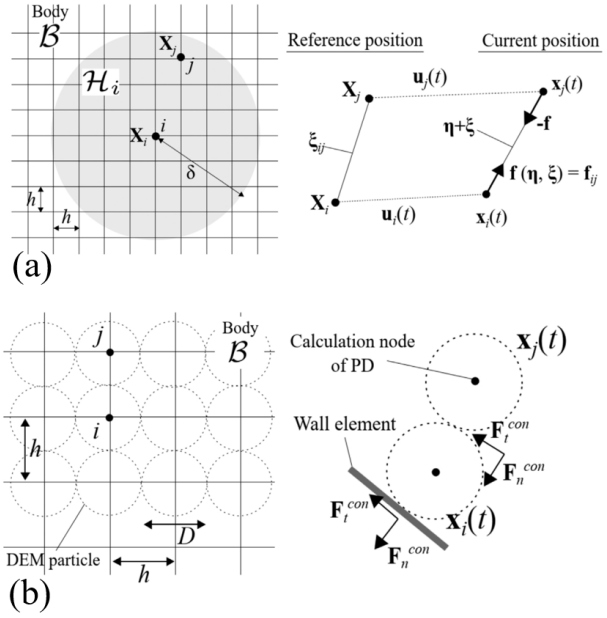

Figure 1. Conceptual diagram of coupled PD-DEM model.

easier to implement. The discretized equation of motion for the computational node i with initial position $\mathbf{X}_i$ at time t is given as follows:

$$m_i\ddot{\mathbf{u}}_i = \sum_{j\in H_i} \boldsymbol{f}(\boldsymbol{\eta},\boldsymbol{\xi})\Delta V_j \Delta V_i + m_i\mathbf{g}. \tag{1}$$

where m is the mass, $\ddot{\mathbf{u}}$ is the acceleration vector, and $\mathbf{f}(\boldsymbol{\eta},\boldsymbol{\xi})$ is the pairwise force function of the bond connecting two nodes, i and j, as shown in Figure 1 (a). The relative displacement vector at the current state is denoted as $\boldsymbol{\eta}$, and the relative position between i and j at the initial configuration is denoted as ξ. ΔV represents the volume of each node and $\mathbf{g}$ is the gravitational acceleration.

In BB-PD, the force density $\mathbf{f}$ is calculated as follows:

$$\boldsymbol{f}(\boldsymbol{\eta},\boldsymbol{\xi}) = cs(\boldsymbol{\eta},\boldsymbol{\xi})\mathbf{M}, \tag{2}$$

where c is the micro-modulus, s is the bond stretch equivalent to the elongation of the distance between nodes, and $\mathbf{M}$ is the

unit vector indicating the direction from $\mathbf{X}_i$ to $\mathbf{X}_j$ after deformation. The value of c depends on the size of the horizon and varies depending on whether 3D conditions, 2D plane stress conditions, or 2D plane strain conditions are used.

While PD can simulate the process from crack initiation to fracture within an object, calculating the interaction forces between objects or fragmented pieces after fracture requires a different approach. Although methods like the short-range force have been proposed to simply prevent penetration after fracture, this study introduced a DEM-based method that accounts for friction, as shown in the following equation:

$$m_i \ddot{\mathbf{u}}_i = \sum_{j \in H_i} \boldsymbol{f}(\boldsymbol{\eta}, \boldsymbol{\xi}) \Delta V_j \Delta V_i + \sum_{j \in C_i} \mathbf{F}_{ij}^{con} + m_i \mathbf{g}. \quad (3)$$

As shown in Figure 1 (b), a sphere with diameter h (equal to the spacing of PD nodes) centered at each PD node was assumed as a DEM particle. Contact calculations based on DEM were applied only when the bond between nodes $\mathbf{X}_i$ and $\mathbf{X}_j$ was broken. In the equation, C means contact conditions, and $\mathbf{F}^{con}$ is the physical contact force, which includes the normal and frictional force. For nodes where all bonds with surrounding nodes are broken, the first term on the right-hand side of the equation becomes zero, resulting in the same translational equation of motion as in standard DEM. For such nodes, torque was calculated for the rotational motion.

2.2 *Bond-softening model*

In PD, the bond between material points $\mathbf{X}_i$ and $\mathbf{X}_j$ is broken when the bond stretch s exceeds a predetermined upper limit (s_0). The proportion of broken bonds among the nodes within the horizon of $\mathbf{X}_i$ is expressed as the local damage index ($\phi(\mathbf{X}_i)$), with a range of 0 to 1, where 1 indicates complete fracture. When using the PMB model, where the magnitude of the force density between nodes is proportional to the bond stretch, it is not possible to obtain the nonlinear stress–strain relationship observed in compacted clay. To solve this problem, this study introduced a bilinear bond softening model, referencing the method of (Niazi et al., 2021). In addition to the bond stretch value (s_c) that determines bond breakage, a threshold bond stretch value (s_1) was introduced to initiate yielding of the force density. The only additional parameter required to improve the PMB model is the one determining the value of s_1.

3 SIMULATION OF DC TEST

3.1 *Experiment of diametral compression test*

The study focuses on the diametral compression test, which is one of the common method to carry out indirect tensile testing. The clay used in these experiments was blue clay as also used by (Shimbo et al., 2022) in their study to perform uniaxial compression experiments. Only specimens with optimal water content were prepared for this test. As shown in Figure 2, initial cracks were made in the specimens with a cutter knife at an angle of 45 degree with respect to horizontal and a length of 15 mm. The results of six tests, as shown in the black plots in the figure, yielded the evolution of the tensile stress with axial strain. The initial slope of the stress-strain curve until the peak tensile stress was approximately the same in all six cases. The tensile strength was obtained in the range of 12 to 15 kPa. From the figure, the cracks gradually propagate from both edges of the initial flaw and eventually their cracks reach the loading surface. In some cases, small cracks were observed starting from the sides of the cylindrical specimens probably due to the inhomogeneities.

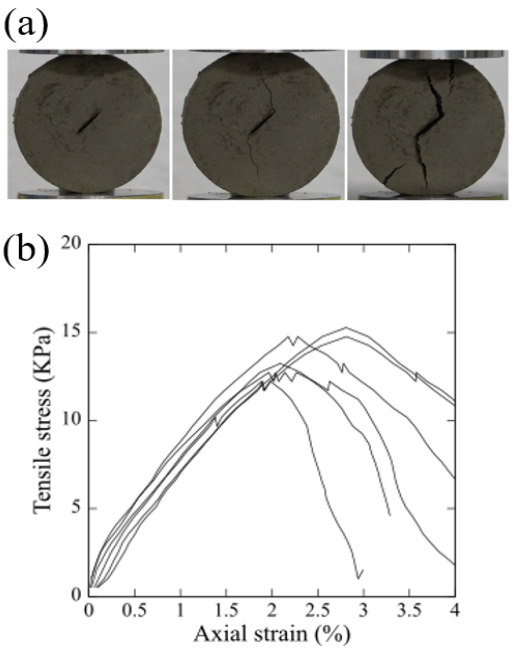

Figure 2. Diametral compression test of compacted clay.

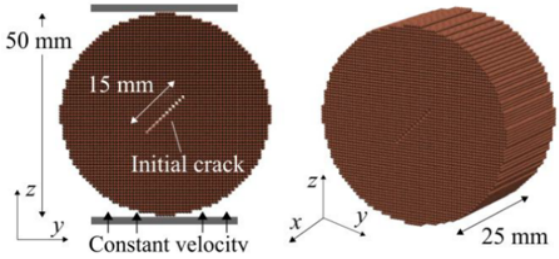

Figure 3. Simulation of diametral compression test.

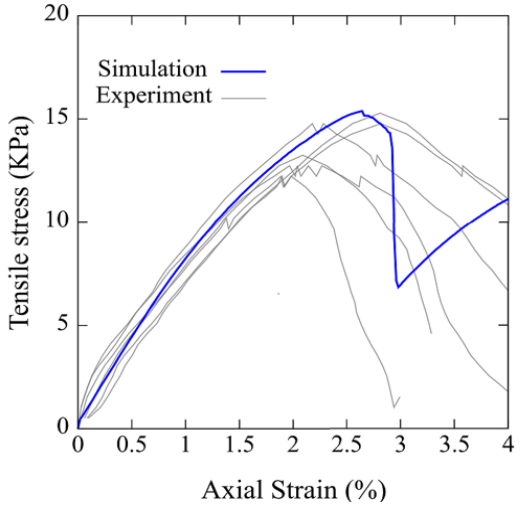

Figure 4. Relationships between tensile stress and axial strain.

3.2 *PD-DEM Simulation*

Figure 3 illustrates the PD model of compacted clay, which comprises of about 100,000 computational nodes, representing a specimen with an approximate height of 50 mm and a thickness of 25 mm akin to the experimental specimens. The parameters were set as follows: $h = 7.8125\times10^{-4}$ m, $\delta = 3h$, the time step was 1.0×10^{-6} s, and the simulation ran for 2.0×10^{6} steps (2.0 seconds). Gravity was applied vertically downward. Compression was applied by displacing the lower wall element in the z-direction at a constant velocity of 0.001 m/s. Young's modulus of 4.5 MPa was chosen as it falls within the typical range for compacted clay specimens. The ultimate tensile strength parameter σ_u and energy release rate G_f for the bond model were set to 18 kPa and 12 J/m², respectively.

The comparison of the simulations with experimental results in terms of the stress-strain relationship and the damage distribution is shown in Figures 4 and 5. The numerical prediction of the stress-strain curve of the proposed bond softening model is shown in Figure 4 as the blue line. The grey plots show the experimental results of six specimens, which is the same as Figure 2 (b). The proposed bond model was in good agreement with the experimental stress-strain relationship. However, the ductile fracture behavior could not be fully reproduced. This point needs to be further improved in the future.

On the other hand, the color bar in Figure 5 represents the damage index (ϕ ($\mathbf{X}_i$)), with colors closer to red indicating greater progression of fracture. Figures 5 (a) to (d) illustrate the progression from an axial strain of 2.64% (near the peak tensile stress) to 2.96% (during the rapid drop in tensile stress). The numerical analysis results confirmed a crack shape connecting the ends of the initial crack to the loading points.

4 SIMULATION OF MULTIPLE CRUSHABLE OBJECTS

To validate the PD-DEM coupled model, a simulation of compressive failure of multiple crushable objects, representing geomaterials like compacted clay, was conducted, as shown in Figure 6. The parameters determined in the previous section were used, assuming compacted clay. Each object, placed in the upper, middle, and lower layers, was identical to the specimen used in the previous section but without the initial crack. The parameters were set as follows: $h = 7.8125\times10^{-4}$ m, $\delta = 3$h, the total number of material points was about 300,000, the time step was 1.0×10^{-6} s, and the simulation ran for 1.0×10^{6} steps (1.0 seconds). Gravity was applied in a downward direction. Compression was applied by displacing the upper wall element in the z-direction at a constant velocity of -0.05 m/s, with a maximum displacement of 50 mm from $z = 150$ mm to $z = 100$ mm. Friction between the wall elements and the objects was set to zero.

Figure 7 shows the simulation results, illustrating the progression of fracture and the distribution of the local damage indices at each time step. Figures 7 (a) to (e) depict the states when the displacement of the upper wall element was 10 to 50 mm. In Figures 7 (a) and (b), cracks first appeared in the object in the lower layer, followed by cracks in the object in the upper layer. In Figure 7 (c), further fracture progressed in the upper and lower objects, and from Figure 7 (d) onward, cracks also appeared in the middle object.

In Figure 8, the distribution of the y-component of the stress tensor, approximated from the force densities inside the horizon, is compared with the distribution of the local damage

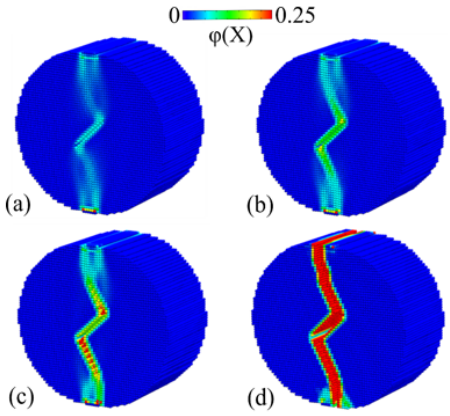

Figure 5. Distributions of local damage indices at (a) 2.64 %, (b) 2.80 %, (c) 2.92 % and (d) 2.96 % of axial strain.

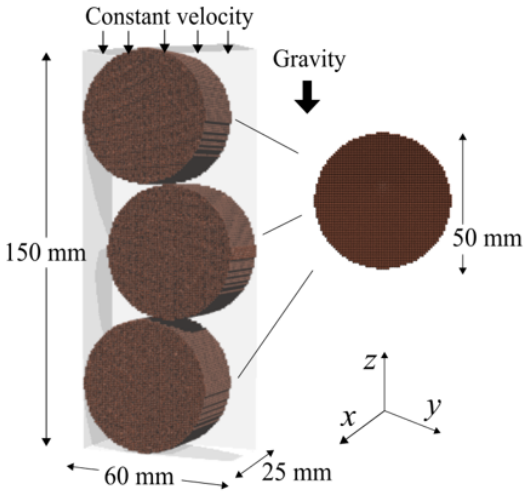

Figure 6. Simulation of compressive failure of multiple crushable objects.

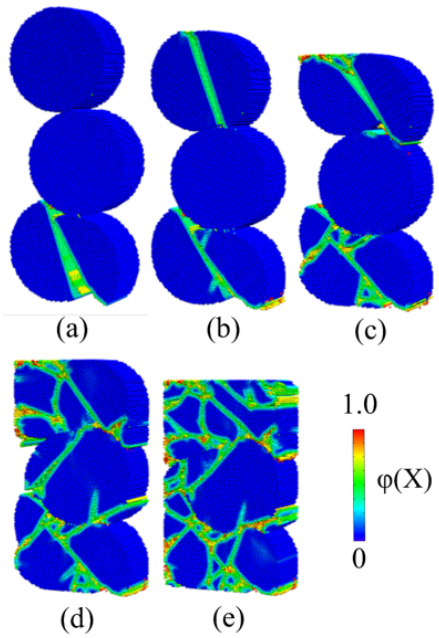

Figure 7. Distributions of local damage indices at various displacements of upper wall.

indices. These represent the state just before cracks appeared in the lower object in Figure 7 (a). In the stress distribution, the red regions indicating tensile stress were more widely distributed within the upper and lower objects compared to the middle object. The damage index distribution also confirmed that fracture began earlier in the upper and lower objects. The sequence of crack initiation observed in Figure 7 was consistent with the stress state within the objects.

5 SUMMARY

The PD-DEM model with the bond softening model was proposed to capture the dynamic fracture behavior of the compacted clay under the 3D condition. The validity of the proposed model was established through the comparison of the simulations with the diametrical compression experiments with an initial flaw. In addition, the proposed model successfully expressed the continuous process of deformation, cracking, and crushing of materials. In future research, the proposed model will be extended to PD with an unstructured grid (Fukumoto et al., 2024) and applying it to engineering problems, such as seismic failure of embankment (Shimbo et al., 2020) and fracture of railway ballasts (Kalyan et al., 2024).

6 ACKNOWLEDGEMENTS

The first and second authors would like to acknowledge the support provided by JSPS (Japan KAKENHI) through Grant Nos. 22K04307 and 24K07672.

7 REFERENCES

Fukumoto, Y., Kalyan, NSSP., Kandasami, RK., Shimbo, T. 2024. Coupled peridynamics and DEM with unstructured grid for evaluating the effect of particle morphology on fracture behavior, *IOP Conference Series: Earth and Environmental Science*, 1480, 012036.

Fukumoto, Y., and Shimbo, T. 2023. 3-D coupled peridynamics and discrete element method for fracture and post-fracture behavior of soil-like materials, *Computers and Geotechnics*, 158, 105372.

Kalyan, NSSP., Fukumoto, Y., Kandasami, RK. 2024. Investigating rock particle breakage using 3D coupled peridynamics-discrete element method: Emphasis on local surface features, *Engineering Fracture Mechanics*, 312, 110585.

Niazi, S., Chen, Z., Bobaru, F. 2021. Crack nucleation in brittle and quasi-brittle materials: A peridynamic analysis. *Theoretical and Applied Fracture Mechanics*, 112, 102855.

Shimbo, T., Itto, R., Inaba, K., Araki, K., Watanabe, N. 2020. Seismic response analysis for ordinary state-based peridynamics in a linear isotropic elastic material. *Journal of Peridynamics and Nonlocal Modeling*, 2, 185-204.

Shimbo, T., Shinzo, C., Uchii, U., Itto, R. Fukumoto, Y. 2022. Effect of different water contents and initial crack lengths on the mechanical properties and failure modes of pre-cracked compacted clay under uniaxial compression, *Engineering Geology*, 301, 106593.

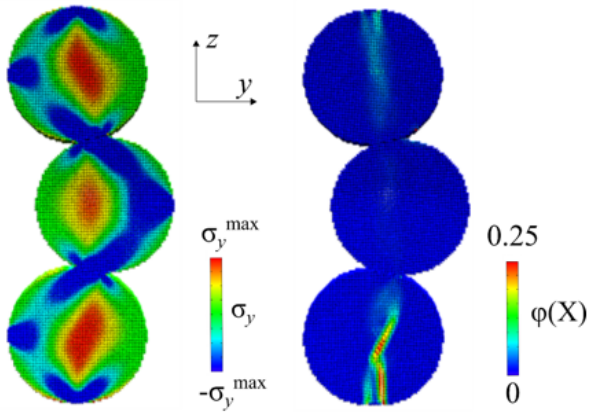

Figure 8. Distribution of stress components σ_y just before fracture and distribution of local damage indices immediately after fracture.